THE JOURNAL OF PHYSICAL CHEMISTRY Letters

Letter

Cite This: J. Phys. Chem. Lett. 2018, 9, 1620−1626

pubs.acs.org/JPCL

Carbene−Metal−Amide Bond Deformation, Rather Than Ligand Rotation, Drives Delayed Fluorescence

Elliot J. Taffet,[†] Yoann Olivier,[‡] Frankie Lam,[†] David Beljonne,[‡] and Gregory D. Scholes*[,†]

[†]Department of Chemistry, Princeton University, Princeton, New Jersey 08544, United States

[‡]Department of Chemistry, University of Mons, 7000 Mons, Belgium

Supporting Information

ABSTRACT: We report three characteristics of ideal thermally activated delayed fluorescence molecular systems apparent in carbene−metal−amides: (a) an exceptionally small singlet−triplet gap that effectively eliminates the thermal activation barrier to reverse intersystem crossing; (b) significant singlet oscillator strength promoting fluorescence in the region of this small barrier; and (c) enlarged spin−orbit coupling driving reverse intersystem crossing in this region. We carry out highly correlated quantum-chemical calculations to detail the relative energies of and spin−orbit couplings between the singlet and triplet states, finding that they fall closer together in energy and couple more strongly in going from the singlet ground-state to the triplet optimized geometry. This structural reorganization is defined not by rotation of the ligands but by a nontrivial bending of the carbene−metal−amide bond angle. This bending reduces carbene−metal−amide symmetry and enhances singlet−triplet interaction strength. We clarify that the reverse intersystem crossing triggering delayed fluorescence occurs around the coplanar triplet geometric optimum.

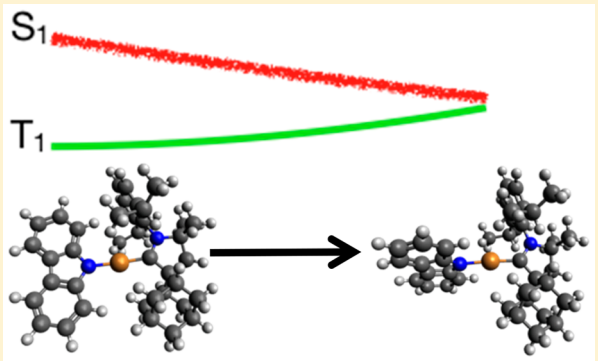

Organic light-emitting diodes (OLEDs) are evaluated based on their capacity to convert electricity to light. In this respect, one state-of-the-art photophysical mechanism has propagated in the OLED literature: delayed fluorescence (DF). DF can convert electronically generated singlet and triplet charge carriers to light—quadrupling the number of photons generated relative to just singlet-state fluorescence. As such, this process enhances conversion efficiency by multiplying the molecular production of light. This process can be realized in molecular systems by reducing the energy gap between singlet and triplet electronic excited states—the exchange energy. The exchange energy is diminished when the electron density migrates between orthogonal units in a molecular assembly following an electronic transition (a charge-transfer excitation), which may, in turn, be accompanied by intersystem crossing (ISC) and reverse intersystem crossing (RISC) from singlet to triplet and triplet to singlet states, respectively. RISC is essential to the realization of efficient DF emitters, since it permits triplet states to recombine radiatively with the ground state in a spin-allowed process.

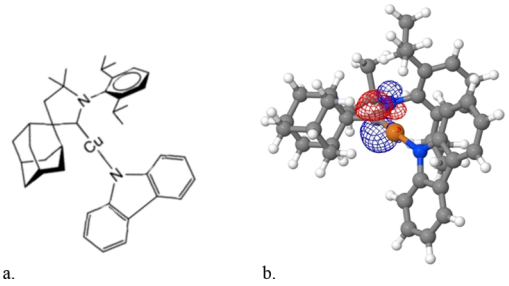

Figure 1. (a) Chemical structure of CMA2. (b) Calculated CMA2 LUMO (isovalue = 0.06). Orbital density is concentrated on the adjacent carbene carbon and nitrogen $2p_z$ orbitals, with an additional nontrivial contribution from the copper metal center.

There have been notable advances in studies of DF recently that have impacted modern-day OLEDs.[1−23] Initially, the efficiency of first-generation fluorescence-based OLEDs was surpassed by second-generation phosphorescence-based (PH)-OLEDs with noble metals, whereby singlet−triplet mixing wrought by spin−orbit coupling rendered emissive triplet excitons populated by electrical stimulation.[24−28] Then these expensive organometallics, featuring less effective blue-light emission,[24] were complemented by OLEDs exhibiting dynamics between triplet and singlet states. The dynamical mechanisms include triplet−triplet annihilation[29,30] and metal−ligand charge-transfer complexes with diminished singlet−triplet energy gaps.[31−36] From these mechanisms, third-generation OLEDs employing triplet-to-singlet thermally activated (TA) DF were espoused.[37−48] These OLEDs included donor−acceptor assemblies with localized CT

Received: February 14, 2018
Accepted: March 14, 2018
Published: March 14, 2018

DOI: 10.1021/acs.jpclett.8b00503
J. Phys. Chem. Lett. 2018, 9, 1620−1626

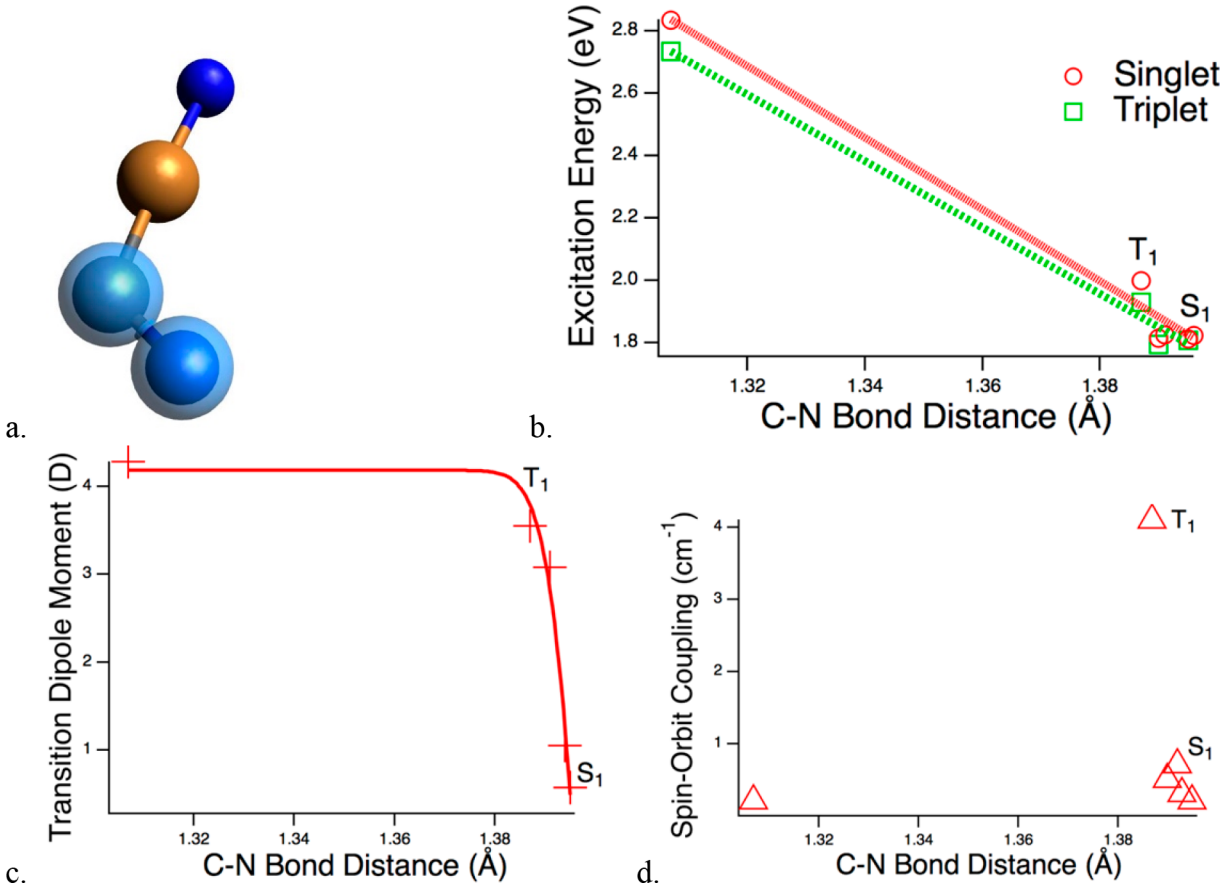

Figure 2. (a) The carbene-metal-amide three-center interaction along with the nitrogen adjacent to the carbon are displayed (all other atoms are omitted for clarity). The two circled atoms represent the carbon−nitrogen bond that is followed along the relaxation pathway from the ground-state to the singlet excited-state optimized geometry. (b) Relationship between excitation energy and C−N bond distance for both the singlet and triplet excited states. The points corresponding to the triplet and singlet optimized geometries are labeled "T_1" and "S_1", respectively. The dotted and dashed lines are guides for the eye reflecting the diminished energy gap. The singlet−triplet energy gap decreases from 0.1 to 0.07 to less than 0.01 eV in going from the ground to the triplet to the singlet optimized geometry. (c) Relationship between transition dipole moment (in Debye, D) and C−N bond distance. The transition dipole moment at the triplet optimized geometry is reduced to 83% of its maximum value, while it drops to 13% of its maximum value at the singlet optimized geometry. A logarithmic fit illustrating the strongly suppressed transition dipole moment stemming from reorganization to the S_1 optimized geometry from T_1 is plotted. (d) Relationship between spin−orbit coupling (in cm^{-1}) and C−N bond distance. The spin−orbit coupling is maximized at the triplet optimized geometry.

excitons stemming from twisted geometries[49,50]—the exciton confinement (small relaxation energy) leading to the realization of efficient blue TADF emitters. Nevertheless, the efficiency of these metal-free OLEDs is curtailed by large singlet−triplet gaps and RISC time constants.

Here, we report on the photophysics of highly efficient DF emitters—carbene−metal−amides (CMA)—that minimize the singlet−triplet gap so as to attenuate the thermal activation barrier to RISC.[51,52] This attenuation, in turn, raises the rate at which triplet excitons radiatively recombine to the ground state via DF, thereby averting bimolecular[53] and nonradiative[52] degradation pathways. There remains the question, however, of the precise CMA geometry that best promotes RISC and subsequent DF. Di et al.[51] proposed a rotationally accessed spin-state *inversion* mechanism—claiming that dynamic relaxation in the singlet excited state pulled its energy *below* that of the triplet state after passing through a point of intersection. An ensuing computational study, however, found no such point of intersection between the states—ligand rotation merely quenches the singlet−triplet exchange energy.[52] We expound upon this computational study by evaluating the effect of the carbene−metal−amide bond angle on the singlet−triplet gap and spin−orbit coupling. We find that triplet-state distortion of this bond angle—being almost perfectly straight in the ground state—greatly enlarges the spin−orbit coupling while having a subtle effect on the singlet−triplet gap. Yet while this gap also shrinks following ligand rotation, a concomitant decrease in the spin−orbit coupling lowers the interaction between singlet and triplet, even as their energies come closer together. This makes fully rotated singlet-state geometries less accessible than coplanar conformations. Thus, while we corroborate the idea of rotationally accessed spin-state *intersection* (a RASI different from that presented originally[51]) due to the asymptotic convergence of singlet and triplet excitation energies at the twisted CMA geometry, we assert that the small singlet−triplet gap at the coplanar triplet geometry, complemented by robust spin−orbit coupling, leads to RISC at nontwisted geometries. These structures have larger singlet-state oscillator strength supporting optimal DF.

We carried out state-averaged CASSCF calculations[54−68] with Slater determinants on copper-centered CMA2 (see Figure 1a)—using *Gaussian 16*[69] and the def2-SVP basis set[70,71]—to evaluate the excitation energies and configurations of both the first triplet and singlet excited states. An active

DOI: 10.1021/acs.jpclett.8b00503
J. Phys. Chem. Lett. 2018, 9, 1620−1626

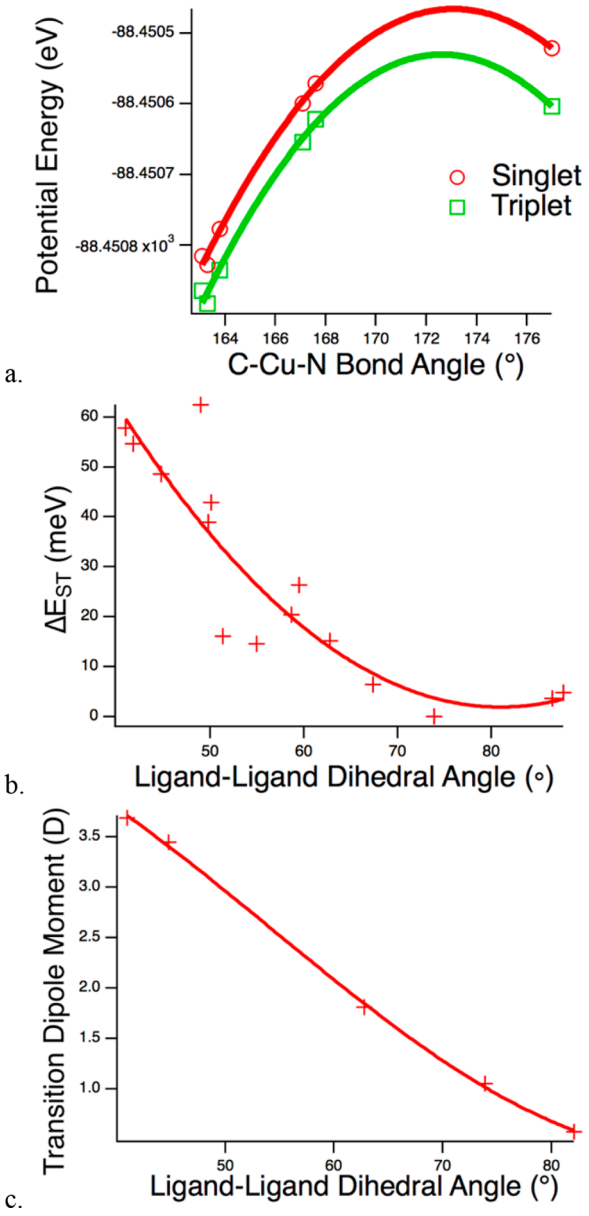

Figure 3. (a) Evolution of the triplet and singlet energies with respect to the carbene−metal−amide bond angle in copper-centered CMA2 along the optimization path from the ground state to the triplet minimum geometry. (b) Evolution of the singlet−triplet energy gap (ΔE_{ST}) in copper-centered CMA2 along the optimization path from the triplet state to the singlet minimum geometry. (c) Evolution of the singlet transition dipole moment along the optimization path from the triplet state to the singlet minimum geometry, fitted sinusoidally as in the work of Di et al.[51]

space of four electrons in four orbitals was utilized due to the predominant HOMO−LUMO nature of both excited states,[52] having confirmed that a marginal difference in excitation energies results from active-space expansion (Figure S1). This was verified with active spaces as large as 16 electrons in 16 orbitals using spin-adapted state-specific Density Matrix Renormalization Group (DMRG)-SCF via the *Block* program.[72−99] We computed the approximate excited-state spin−orbit coupling[100] within our state-averaged CASSCF implementation. These electronic structure calculations are based on geometries optimized using DFT/TDDFT without[51] and with the Tamm−Dancoff Approximation,[101−103] finding negligible differences in structure and excitation energies with respect to the method—underscoring the lack of triplet instability for TDDFT[104−106] on CMA2 (Table S1). Using the successive iterations along the excited-state optimization paths from the ground state to the triplet and from the triplet to the singlet, we construct relative potential-energy curves of the excited states.

The lowest-lying singlet and triplet excited states of CMA2 are charge-transfer in nature. As shown in Figure 1b, the prominent ligand contribution to the CMA2 lowest unoccupied molecular orbital (LUMO) is from the carbene carbon and adjacent nitrogen $2p_z$ orbitals aligned out of phase, which means that the two atoms are repelled from each other in the excited state.

This was verified by wave function configuration analysis at each optimized geometry, with 90% of the singlet wave function comprised of LUMO one-particle excitation (Figure S2). As the singlet relaxes, the strength of the antibonding interaction is mitigated by C−N bond stretching, which, in turn, pushes the LUMO down in energy. For this reason, the C−N bond displayed in Figure 2a is followed from the ground to the relaxed singlet geometry. Relevant normal modes at this minimum-energy point are enumerated in Table S2. Figures 2b, 2c and 2d detail the change in excitation energy, singlet excited-state transition dipole moment, and triplet-singlet excited-state spin−orbit coupling, respectively, with respect to C−N bond elongation.

While a subtle elongation of the C−N bond from the triplet to the singlet optimized geometries leads to near-degeneracy of the excited states, the oscillator strength and spin−orbit coupling become significantly suppressed at the singlet optimized geometry. The transition dipole moment and spin−orbit coupling decrease by factors of seven and 20, respectively, in going from T_1 to S_1. Moreover, the reduction in the singlet−triplet gap is just 0.06 eV, from 0.07 eV at T_1 to 0.01 eV at S_1. These results suggest that the geometries leading to DF hover around the T_1 optimum as originally suggested by Di et al.[51] The small energy gap from triplet to singlet at this geometry, along with enhanced spin−orbit coupling, help to facilitate RISC, and the planarity of the ligands helps to sustain oscillator strength close to that of the ground state.

Given the likelihood of DF occurring near the minimum of the T_1 potential-energy surface, we resolve this surface in Figure 3a by considering the change in carbene−metal−amide bond angle over the course of the T_1 geometry optimization.

Like the carbon−nitrogen bond, the carbon−copper−nitrogen bond angle distorts during excited-state relaxation due to the antibonding interaction between the metal d_{xz} orbital and the carbon $2p_z$ orbital. This symmetry breaking of the carbene-metal-amide bond axis leads to greater spin−orbit coupling and, in turn, greater interaction between the singlet and triplet states. While almost perfectly flat (177 degrees) in the ground state, an apparent "kink" at the T_1 optimized geometry lowers the bond angle to 163 degrees. This "kink" decouples the ligands appended to each side of the metal, thereby serving to lower the singlet−triplet gap as displayed in Figure 3a. Nonetheless, both excited states are stabilized significantly by this structural distortion. The singlet state is less significantly stabilized by ligand rotation to an orthogonal orientation at the singlet excited-state geometry, which further decouples the ligands and collapses the singlet−triplet gap (Figure 3b). This collapse, but not inversion, was further verified by carrying out state-averaged CASSCF with scalar relativistic effects using the *X2C* module in *PySCF*.[107−109] An

DOI: 10.1021/acs.jpclett.8b00503
J. Phys. Chem. Lett. 2018, 9, 1620−1626

energy gap of 4 meV was obtained, compared to 4.6 meV without relativistic effects (Table S3). As this gap asymptotically converges to zero when the ligands are rotated perpendicular to each other, we describe this phenomenon as rotationally accessed spin-state *intersection* that counterintuitively limits DF, as Figures 2d and 3c reveal. For one, RISC depends directly on spin−orbit coupling—which returns to the ground-state value at S_1 as the carbon, copper, and nitrogen atoms realign (bond angle of 175 degrees)—and not ΔE_{ST}. Moreover, RISC is followed by fluorescence with efficiency directly dependent on oscillator strength. Since the singlet potential-energy surface is relatively flat in the region from T_1 to S_1,[52] there does not appear to be a strong thermodynamic driving force inducing rotation and, in turn, delayed-fluorescence quenching, in CMA2. On the other hand, the excited singlet is driven toward the near-resonant excited triplet minimum-energy geometry by enlarged spin−orbit coupling mediating intersystem crossing, meaning that singlet-state population should be concentrated around this seam. As such, the thermodynamic accessibility of the triplet optimized geometry should serve to hinder full ligand rotation in the singlet excited state, which itself hinders delayed-fluorescence efficacy (see Supporting Information).

In conclusion, coplanar carbene−metal−amide structures achieve the trifecta of small singlet−triplet gaps, large oscillator strengths, and large spin−orbit couplings. The rotationally accessed point of intersection between the singlet and triplet excited states is a moot point, since ligand rotation only marginally affects the singlet−triplet gap and is deleterious to DF in the context of spin−orbit coupling and singlet oscillator strength. Rather, carbene−metal−amide bond deformation, accompanied by carbene carbon−nitrogen bond stretching, are shown to be the crucial coordinates leading to an optimized triplet geometry with maximal spin−orbit coupling and over 80% of the ground-state oscillator strength. This is explained by the fact that the lowest triplet excitation in CMA2 primarily involves the LUMO, characterized by carbon−nitrogen and carbon−copper antibonding interactions. DF is predicted to occur efficiently in CMA2 because, while the driving force for these distortions is large, the driving force for ligand rotation is small. Increasing sterics and solvent viscosity—effectively emulating the hindered ligand rotation in the solid state—should further increase the efficiency of CMA DF in solution.

■ ASSOCIATED CONTENT

Supporting Information

The Supporting Information is available free of charge on the ACS Publications website at DOI: 10.1021/acs.jpclett.8b00503.

Sensitivity of the computed singlet−triplet gap to active-space size, fractional contribution of the HOMO−LUMO single-electron excitation at each geometry, comparison of singlet−triplet gaps computed using TDDFT with and without the Tamm−Dancoff Approximation, relevant twisting/bending/stretching vibrational modes (with corresponding animations), comparison of singlet−triplet gaps using state-averaged CASSCF with and without scalar relativistic effects, and an explication of how the coplanar triplet optimized geometry impedes full ligand rotation in the singlet excited state (PDF)

Out-of-plane ligand twisting animation (AVI)

Bending carbon−copper−nitrogen bond angle animation (AVI)

Stretching carbene carbon−nitrogen bond animation (AVI)

■ AUTHOR INFORMATION

Corresponding Author

*E-mail: gscholes@princeton.edu.

ORCID

Elliot J. Taffet: 0000-0002-8321-5116

Gregory D. Scholes: 0000-0003-3336-7960

Notes

The authors declare no competing financial interest.

■ ACKNOWLEDGMENTS

The authors would like to thank Dan Credgington for useful discussion. This work was supported by Princeton University through the Innovation Fund for New Ideas in the Natural Sciences. This project has received funding from the European Union Horizon 2020 research and innovation programme under Grant Agreement No. 646176 (EXTMOS). D.B. and Y.O. would like to acknowledge the Belgian National Fund for Scientific Research (FNRS/F.R.S.) for financial support. D.B. is a FNRS Research Director.

■ REFERENCES

(1) Tang, C. W.; VanSlyke, S. A. Organic Electroluminescent Diodes. *Appl. Phys. Lett.* **1987**, *51*, 913−915.

(2) Burroughes, J.; Bradley, D.; Brown, A.; Marks, R.; Mackay, K.; Friend, R.; Burns, P.; Holmes, A. Light-Emitting Diodes Based on Conjugated Polymers. *Nature* **1990**, *347*, 539−541.

(3) Peng, Q.; Fan, D.; Duan, R.; Yi, Y.; Niu, Y.; Wang, D.; Shuai, Z. Theoretical Study of Conversion and Decay Processes of Excited Triplet and Singlet States in a Thermally Activated Delayed Fluorescence Molecule. *J. Phys. Chem. C* **2017**, *121*, 13448−13456.

(4) dos Santos, P. L.; Ward, J. S.; Batsanov, A. S.; Bryce, M. R.; Monkman, A. P. Optical and Polarity Control of Donor−Acceptor Conformation and Their Charge-Transfer States in Thermally Activated Delayed-Fluorescence Molecules. *J. Phys. Chem. C* **2017**, *121*, 16462−16469.

(5) Shafikov, M. Z.; Suleymanova, A.; Schinabeck, A.; Yersin, H. Dinuclear Ag (I) Complex Designed for Highly Efficient Thermally Activated Delayed Fluorescence. *J. Phys. Chem. Lett.* **2018**, *9*, 702.

(6) Rajamalli, P.; Senthilkumar, N.; Huang, P.-Y.; Ren-Wu, C.-C.; Lin, H.-W.; Cheng, C.-H. New Molecular Design Concurrently Providing Superior Pure Blue, Thermally Activated Delayed Fluorescence and Optical out-Coupling Efficiencies. *J. Am. Chem. Soc.* **2017**, *139*, 10948−10951.

(7) Shao, S.; Hu, J.; Wang, X.; Wang, L.; Jing, X.; Wang, F. Blue Thermally Activated Delayed Fluorescence Polymers with Non-conjugated Backbone and through-Space Charge Transfer Effect. *J. Am. Chem. Soc.* **2017**, *139*, 17739−17742.

(8) Komatsu, R.; Ohsawa, T.; Sasabe, H.; Nakao, K.; Hayasaka, Y.; Kido, J. Manipulating the Electronic Excited State Energies of Pyrimidine-Based Thermally Activated Delayed Fluorescence Emitters to Realize Efficient Deep-Blue Emission. *ACS Appl. Mater. Interfaces* **2017**, *9*, 4742−4749.

(9) Sun, H.; Hu, Z.; Zhong, C.; Chen, X.; Sun, Z.; Brédas, J.-L. Impact of Dielectric Constant on the Singlet−Triplet Gap in Thermally Activated Delayed Fluorescence Materials. *J. Phys. Chem. Lett.* **2017**, *8*, 2393−2398.

(10) Tsujimoto, H.; Ha, D.-G.; Markopoulos, G.; Chae, H. S.; Baldo, M. A.; Swager, T. M. Thermally Activated Delayed Fluorescence and Aggregation Induced Emission with through-Space Charge Transfer. *J. Am. Chem. Soc.* **2017**, *139*, 4894−4900.

(11) Jürgensen, N.; Kretzschmar, A.; Höfle, S.; Freudenberg, J.; Bunz, U. H.; Hernandez-Sosa, G. Sulfone-Based Deep Blue Thermally

DOI: 10.1021/acs.jpclett.8b00503
J. Phys. Chem. Lett. 2018, 9, 1620−1626

Activated Delayed Fluorescence Emitters: Solution-Processed Organic Light-Emitting Diodes with High Efficiency and Brightness. *Chem. Mater.* **2017**, *29*, 9154−9161.
(12) Samanta, P. K.; Kim, D.; Coropceanu, V.; Bredas, J.-L. Up-Conversion Intersystem Crossing Rates in Organic Emitters for Thermally Activated Delayed Fluorescence: Impact of the Nature of Singlet Vs Triplet Excited States. *J. Am. Chem. Soc.* **2017**, *139*, 4042−4051.
(13) Im, Y.; Kim, M.; Cho, Y. J.; Seo, J.-A.; Yook, K. S.; Lee, J. Y. Molecular Design Strategy of Organic Thermally Activated Delayed Fluorescence Emitters. *Chem. Mater.* **2017**, *29*, 1946−1963.
(14) Zhou, T.; Xie, G.; Gong, S.; Huang, M.; Luo, J.; Yang, C. Simple Incl3 Doped Pedot: Pss and Uv−Ozone Treatment Strategy: External Quantum Efficiency up to 21% for Solution-Processed Organic Light-Emitting Devices with a Thermally Activated Delayed Fluorescence Emitter. *ACS Appl. Mater. Interfaces* **2017**, *9*, 34139−34145.
(15) Ryoo, C. H.; Cho, I.; Han, J.; Yang, J.-h.; Kwon, J. E.; Kim, S.; Jeong, H.; Lee, C.; Park, S. Y. Structure−Property Correlation in Luminescent Indolo [3, 2-B] Indole (Idid) Derivatives: Unraveling the Mechanism of High Efficiency Thermally Activated Delayed Fluorescence (Tadf). *ACS Appl. Mater. Interfaces* **2017**, *9*, 41413−41420.
(16) Lin, C.-C.; Huang, M.-J.; Chiu, M.-J.; Huang, M.-P.; Chang, C.-C.; Liao, C.-Y.; Chiang, K.-M.; Shiau, Y.-J.; Chou, T.-Y.; Chu, L.-K.; et al. Molecular Design of Highly Efficient Thermally Activated Delayed Fluorescence Hosts for Blue Phosphorescent and Fluorescent Organic Light-Emitting Diodes. *Chem. Mater.* **2017**, *29*, 1527−1537.
(17) Cui, L. S.; Nomura, H.; Geng, Y.; Kim, J. U.; Nakanotani, H.; Adachi, C. Controlling Singlet−Triplet Energy Splitting for Deep-Blue Thermally Activated Delayed Fluorescence Emitters. *Angew. Chem.* **2017**, *129*, 1593−1597.
(18) Freeman, D. M.; Musser, A. J.; Frost, J. M.; Stern, H. L.; Forster, A. K.; Fallon, K. J.; Rapidis, A. G.; Cacialli, F.; McCulloch, I.; Clarke, T. M.; et al. Synthesis and Exciton Dynamics of Donor-Orthogonal Acceptor Conjugated Polymers: Reducing the Singlet−Triplet Energy Gap. *J. Am. Chem. Soc.* **2017**, *139*, 11073−11080.
(19) Mamada, M.; Inada, K.; Komino, T.; Potscavage, W. J., Jr; Nakanotani, H.; Adachi, C. Highly Efficient Thermally Activated Delayed Fluorescence from an Excited-State Intramolecular Proton Transfer System. *ACS Cent. Sci.* **2017**, *3*, 769−777.
(20) Chen, J.-X.; Liu, W.; Zheng, C.-J.; Wang, K.; Liang, K.; Shi, Y.-Z.; Ou, X.-M.; Zhang, X.-H. Coumarin-Based Thermally Activated Delayed Fluorescence Emitters with High External Quantum Efficiency and Low Efficiency Roll-Off in the Devices. *ACS Appl. Mater. Interfaces* **2017**, *9*, 8848−8854.
(21) Sasabe, H.; Hayasaka, Y.; Komatsu, R.; Nakao, K.; Kido, J. Highly Luminescent Π-Conjugated Terpyridine Derivatives Exhibiting Thermally Activated Delayed Fluorescence. *Chem. - Eur. J.* **2017**, *23*, 114−119.
(22) Chen, X. K.; Tsuchiya, Y.; Ishikawa, Y.; Zhong, C.; Adachi, C.; Brédas, J. L. A New Design Strategy for Efficient Thermally Activated Delayed Fluorescence Organic Emitters: From Twisted to Planar Structures. *Adv. Mater.* **2017**, *29*, 1702767.
(23) Zhang, D.; Zhao, C.; Zhang, Y.; Song, X.; Wei, P.; Cai, M.; Duan, L. Highly Efficient Full-Color Thermally Activated Delayed Fluorescent Organic Light-Emitting Diodes: Extremely Low Efficiency Roll-Off Utilizing a Host with Small Singlet−Triplet Splitting. *ACS Appl. Mater. Interfaces* **2017**, *9*, 4769−4777.
(24) Zhang, Q.; Li, B.; Huang, S.; Nomura, H.; Tanaka, H.; Adachi, C. Efficient Blue Organic Light-Emitting Diodes Employing Thermally Activated Delayed Fluorescence. *Nat. Photonics* **2014**, *8*, 326−332.
(25) Adachi, C.; Baldo, M. A.; Thompson, M. E.; Forrest, S. R. Nearly 100% Internal Phosphorescence Efficiency in an Organic Light-Emitting Device. *J. Appl. Phys.* **2001**, *90*, 5048−5051.
(26) Yersin, H. *Highly Efficient Oleds with Phosphorescent Materials*; John Wiley & Sons: Weinheim, Germany, 2008.
(27) Baldo, M. A.; O'brien, D.; You, Y.; Shoustikov, A.; Sibley, S.; Thompson, M.; Forrest, S. Highly Efficient Phosphorescent Emission from Organic Electroluminescent Devices. *Nature* **1998**, *395*, 151−154.
(28) Ma, Y.; Zhang, H.; Shen, J.; Che, C. Electroluminescence from Triplet Metal—Ligand Charge-Transfer Excited State of Transition Metal Complexes. *Synth. Met.* **1998**, *94*, 245−248.
(29) Ganzorig, C.; Fujihira, M. A Possible Mechanism for Enhanced Electrofluorescence Emission through Triplet−Triplet Annihilation in Organic Electroluminescent Devices. *Appl. Phys. Lett.* **2002**, *81*, 3137−3139.
(30) Kondakov, D.; Pawlik, T.; Hatwar, T.; Spindler, J. Triplet Annihilation Exceeding Spin Statistical Limit in Highly Efficient Fluorescent Organic Light-Emitting Diodes. *J. Appl. Phys.* **2009**, *106*, 124510.
(31) Zhang, Q.; Zhou, Q.; Cheng, Y.; Wang, L.; Ma, D.; Jing, X.; Wang, F. Highly Efficient Electroluminescence from Green-Light-Emitting Electrochemical Cells Based on Cui Complexes. *Adv. Funct. Mater.* **2006**, *16*, 1203−1208.
(32) Tsuboyama, A.; Kuge, K.; Furugori, M.; Okada, S.; Hoshino, M.; Ueno, K. Photophysical Properties of Highly Luminescent Copper (I) Halide Complexes Chelated with 1, 2-Bis (Diphenylphosphino) Benzene. *Inorg. Chem.* **2007**, *46*, 1992−2001.
(33) Hashimoto, M.; Igawa, S.; Yashima, M.; Kawata, I.; Hoshino, M.; Osawa, M. Highly Efficient Green Organic Light-Emitting Diodes Containing Luminescent Three-Coordinate Copper (I) Complexes. *J. Am. Chem. Soc.* **2011**, *133*, 10348−10351.
(34) Hsu, C.-W.; Lin, C.-C.; Chung, M.-W.; Chi, Y.; Lee, G.-H.; Chou, P.-T.; Chang, C.-H.; Chen, P.-Y. Systematic Investigation of the Metal-Structure−Photophysics Relationship of Emissive D10-Complexes of Group 11 Elements: The Prospect of Application in Organic Light Emitting Devices. *J. Am. Chem. Soc.* **2011**, *133*, 12085−12099.
(35) Zhang, Q.; Komino, T.; Huang, S.; Matsunami, S.; Goushi, K.; Adachi, C. Triplet Exciton Confinement in Green Organic Light-Emitting Diodes Containing Luminescent Charge-Transfer Cu (I) Complexes. *Adv. Funct. Mater.* **2012**, *22*, 2327−2336.
(36) Deaton, J. C.; Switalski, S. C.; Kondakov, D. Y.; Young, R. H.; Pawlik, T. D.; Giesen, D. J.; Harkins, S. B.; Miller, A. J. M.; Mickenberg, S. F.; Peters, J. C. E-Type Delayed Fluorescence of a Phosphine-Supported Cu2(M-Nar2)2 Diamond Core: Harvesting Singlet and Triplet Excitons in Oleds. *J. Am. Chem. Soc.* **2010**, *132*, 9499−9508.
(37) Endo, A.; Sato, K.; Yoshimura, K.; Kai, T.; Kawada, A.; Miyazaki, H.; Adachi, C. Efficient Up-Conversion of Triplet Excitons into a Singlet State and Its Application for Organic Light Emitting Diodes. *Appl. Phys. Lett.* **2011**, *98*, 083302.
(38) Goushi, K.; Yoshida, K.; Sato, K.; Adachi, C. Organic Light-Emitting Diodes Employing Efficient Reverse Intersystem Crossing for Triplet-to-Singlet State Conversion. *Nat. Photonics* **2012**, *6*, 253−258.
(39) Nakagawa, T.; Ku, S.-Y.; Wong, K.-T.; Adachi, C. Electroluminescence Based on Thermally Activated Delayed Fluorescence Generated by a Spirobifluorene Donor−Acceptor Structure. *Chem. Commun.* **2012**, *48*, 9580−9582.
(40) Méhes, G.; Nomura, H.; Zhang, Q.; Nakagawa, T.; Adachi, C. Enhanced Electroluminescence Efficiency in a Spiro-Acridine Derivative through Thermally Activated Delayed Fluorescence. *Angew. Chem., Int. Ed.* **2012**, *51*, 11311−11315.
(41) Youn Lee, S.; Yasuda, T.; Nomura, H.; Adachi, C. High-Efficiency Organic Light-Emitting Diodes Utilizing Thermally Activated Delayed Fluorescence from Triazine-Based Donor−Acceptor Hybrid Molecules. *Appl. Phys. Lett.* **2012**, *101*, 093306.
(42) Zhang, Q.; Li, J.; Shizu, K.; Huang, S.; Hirata, S.; Miyazaki, H.; Adachi, C. Design of Efficient Thermally Activated Delayed Fluorescence Materials for Pure Blue Organic Light Emitting Diodes. *J. Am. Chem. Soc.* **2012**, *134*, 14706−14709.
(43) Tanaka, H.; Shizu, K.; Miyazaki, H.; Adachi, C. Efficient Green Thermally Activated Delayed Fluorescence (Tadf) from a Phenoxazine−Triphenyltriazine (Pxz−Trz) Derivative. *Chem. Commun.* **2012**, *48*, 11392−11394.

DOI: 10.1021/acs.jpclett.8b00503
J. Phys. Chem. Lett. 2018, 9, 1620−1626

(44) Uoyama, H.; Goushi, K.; Shizu, K.; Nomura, H.; Adachi, C. Highly Efficient Organic Light-Emitting Diodes from Delayed Fluorescence. *Nature* **2012**, *492*, 234−238.
(45) Li, J.; Nakagawa, T.; Macdonald, J.; Zhang, Q.; Nomura, H.; Miyazaki, H.; Adachi, C. Highly Efficient Organic Light-Emitting Diode Based on a Hidden Thermally Activated Delayed Fluorescence Channel in a Heptazine Derivative. *Adv. Mater.* **2013**, *25*, 3319−3323.
(46) Lee, J.; Shizu, K.; Tanaka, H.; Nomura, H.; Yasuda, T.; Adachi, C. Oxadiazole-and Triazole-Based Highly-Efficient Thermally Activated Delayed Fluorescence Emitters for Organic Light-Emitting Diodes. *J. Mater. Chem. C* **2013**, *1*, 4599−4604.
(47) Wu, S.; Aonuma, M.; Zhang, Q.; Huang, S.; Nakagawa, T.; Kuwabara, K.; Adachi, C. High-Efficiency Deep-Blue Organic Light-Emitting Diodes Based on a Thermally Activated Delayed Fluorescence Emitter. *J. Mater. Chem. C* **2014**, *2*, 421−424.
(48) Tao, Y.; Yuan, K.; Chen, T.; Xu, P.; Li, H.; Chen, R.; Zheng, C.; Zhang, L.; Huang, W. Thermally Activated Delayed Fluorescence Materials Towards the Breakthrough of Organoelectronics. *Adv. Mater.* **2014**, *26*, 7931−7958.
(49) Rettig, W.; Chandross, E. A. Dual Fluorescence of 4, 4′-Dimethylamino-and 4, 4′-Diaminophenyl Sulfone. Consequences of D-Orbital Participation in the Intramolecular Charge Separation Process. *J. Am. Chem. Soc.* **1985**, *107*, 5617−5624.
(50) Grabowski, Z. R.; Rotkiewicz, K.; Rettig, W. Structural Changes Accompanying Intramolecular Electron Transfer: Focus on Twisted Intramolecular Charge-Transfer States and Structures. *Chem. Rev.* **2003**, *103*, 3899−4032.
(51) Di, D.; et al. High-Performance Light-Emitting Diodes Based on Carbene-Metal-Amides. *Science* **2017**, *356*, 159−163.
(52) Föller, J.; Marian, C. M. Rotationally Assisted Spin-State Inversion in Carbene−Metal−Amides Is an Artifact. *J. Phys. Chem. Lett.* **2017**, *8*, 5643−5647.
(53) Giebink, N.; Forrest, S. Quantum Efficiency Roll-Off at High Brightness in Fluorescent and Phosphorescent Organic Light Emitting Diodes. *Phys. Rev. B: Condens. Matter Mater. Phys.* **2008**, *77*, 235215.
(54) Hegarty, D.; Robb, M. A. Application of Unitary Group Methods to Configuration Interaction Calculations. *Mol. Phys.* **1979**, *38*, 1795−1812.
(55) Eade, R. H. A.; Robb, M. A. Direct Minimization in Mc Scf Theory. The Quasi-Newton Method. *Chem. Phys. Lett.* **1981**, *83*, 362−368.
(56) Schlegel, H. B.; Robb, M. A. Mc Scf Gradient Optimization of the H2co→H2 + Co Transition Structure. *Chem. Phys. Lett.* **1982**, *93*, 43−46.
(57) Bernardi, F.; Bottoni, A.; McDouall, J. J. W.; Robb, M. A.; Schlegel, H. B. Mcscf Gradient Calculation of Transition Structures in Organic Reactions. *Faraday Symp. Chem. Soc.* **1984**, *19*, 137−147.
(58) Frisch, M.; Ragazos, I. N.; Robb, M. A.; Bernhard Schlegel, H. An Evaluation of Three Direct Mc-Scf Procedures. *Chem. Phys. Lett.* **1992**, *189*, 524−528.
(59) Yamamoto, N.; Vreven, T.; Robb, M. A.; Frisch, M. J.; Bernhard Schlegel, H. A Direct Derivative Mc-Scf Procedure. *Chem. Phys. Lett.* **1996**, *250*, 373−378.
(60) Siegbahn, P. E. M. A New Direct Ci Method for Large Ci Expansions in a Small Orbital Space. *Chem. Phys. Lett.* **1984**, *109*, 417−423.
(61) Klene, M.; Robb, M. A.; Frisch, M. J.; Celani, P. Parallel Implementation of the Ci-Vector Evaluation in Full Ci/Cas-Scf. *J. Chem. Phys.* **2000**, *113*, 5653−5665.
(62) Bernardi, F.; Bottoni, A.; Field, M. J.; Guest, M. F.; Hillier, I. H.; Robb, M. A.; Venturini, A. Mc-Scf Study of the Diels-Alder Reaction between Ethylene and Butadiene. *J. Am. Chem. Soc.* **1988**, *110*, 3050−3055.
(63) Bernardi, F.; Bottoni, A.; Olivucci, M.; Robb, M. A.; Schlegel, H. B.; Tonachini, G. Do Supra-Antara Paths Really Exist for 2 + 2 Cycloaddition Reactions? Analytical Computation of the Mc-Scf Hessians for Transition States of Ethylene with Ethylene, Singlet Oxygen, and Ketene. *J. Am. Chem. Soc.* **1988**, *110*, 5993−5995.
(64) Bernardi, F.; Bottoni, A.; Robb, M. A.; Venturini, A. Mcscf Study of the Cycloaddition Reaction between Ketene and Ethylene. *J. Am. Chem. Soc.* **1990**, *112*, 2106−2114.
(65) Tonachini, G.; Schlegel, H. B.; Bernardi, F.; Robb, M. A. Mc-Scf Study of the Addition Reaction of the 1.Delta.G Oxygen Molecule to Ethene. *J. Am. Chem. Soc.* **1990**, *112*, 483−491.
(66) Palmer, I. J.; Olivucci, M.; Bernardi, F.; Robb, M. A. An Mc-Scf Study of the Thermal and Photochemical Cycloaddition of Dewar Benzene. *J. Org. Chem.* **1992**, *57*, 5081−5087.
(67) Palmer, I. J.; Ragazos, I. N.; Bernardi, F.; Olivucci, M.; Robb, M. A. An Mc-Scf Study of the (Photochemical) Paterno-Buchi Reaction. *J. Am. Chem. Soc.* **1994**, *116*, 2121−2132.
(68) Vreven, T.; Bernardi, F.; Garavelli, M.; Olivucci, M.; Robb, M. A.; Schlegel, H. B. Ab Initio Photoisomerization Dynamics of a Simple Retinal Chromophore Model. *J. Am. Chem. Soc.* **1997**, *119*, 12687−12688.
(69) Frisch, M. J., et al. *Gaussian 16*; Gaussian, Inc.: Wallingford, CT, 2016.
(70) Weigend, F.; Häser, M.; Patzelt, H.; Ahlrichs, R. Ri-Mp2: Optimized Auxiliary Basis Sets and Demonstration of Efficiency. *Chem. Phys. Lett.* **1998**, *294*, 143−152.
(71) Weigend, F.; Ahlrichs, R. Balanced Basis Sets of Split Valence, Triple Zeta Valence and Quadruple Zeta Valence Quality for H to Rn: Design and Assessment of Accuracy. *Phys. Chem. Chem. Phys.* **2005**, *7*, 3297−3305.
(72) White, S. R. Density Matrix Formulation for Quantum Renormalization Groups. *Phys. Rev. Lett.* **1992**, *69*, 2863−2866.
(73) White, S. R. Density-Matrix Algorithms for Quantum Renormalization Groups. *Phys. Rev. B: Condens. Matter Mater. Phys.* **1993**, *48*, 10345−10356.
(74) White, S. R.; Martin, R. L. Ab Initio Quantum Chemistry Using the Density Matrix Renormalization Group. *J. Chem. Phys.* **1999**, *110*, 4127−4130.
(75) Daul, S.; Ciofini, I.; Daul, C.; White, S. R. Full-Ci Quantum Chemistry Using the Density Matrix Renormalization Group. *Int. J. Quantum Chem.* **2000**, *79*, 331−342.
(76) White, S. R. Density Matrix Renormalization Group Algorithms with a Single Center Site. *Phys. Rev. B: Condens. Matter Mater. Phys.* **2005**, *72*, 180403.
(77) Rommer, S.; Östlund, S. Class of Ansatz Wave Functions for One-Dimensional Spin Systems and Their Relation to the Density Matrix Renormalization Group. *Phys. Rev. B: Condens. Matter Mater. Phys.* **1997**, *55*, 2164.
(78) Östlund, S.; Rommer, S. Thermodynamic Limit of Density Matrix Renormalization. *Phys. Rev. Lett.* **1995**, *75*, 3537−3540.
(79) Mitrushenkov, A. O.; Linguerri, R.; Palmieri, P.; Fano, G. Quantum Chemistry Using the Density Matrix Renormalization Group Ii. *J. Chem. Phys.* **2003**, *119*, 4148−4158.
(80) Mitrushenkov, A. O.; Fano, G.; Ortolani, F.; Linguerri, R.; Palmieri, P. Quantum Chemistry Using the Density Matrix Renormalization Group. *J. Chem. Phys.* **2001**, *115*, 6815−6821.
(81) Chan, G. K.-L.; Head-Gordon, M. Highly Correlated Calculations with a Polynomial Cost Algorithm: A Study of the Density Matrix Renormalization Group. *J. Chem. Phys.* **2002**, *116*, 4462−4476.
(82) Legeza, Ö.; Sólyom, J. Optimizing the Density-Matrix Renormalization Group Method Using Quantum Information Entropy. *Phys. Rev. B: Condens. Matter Mater. Phys.* **2003**, *68*, 195116.
(83) Legeza, Ö.; RÖDer, J.; Hess, B. A. Qc-Dmrg Study of the Ionic-Neutral Curve Crossing of Lif. *Mol. Phys.* **2003**, *101*, 2019−2028.
(84) Li, Z.; Chan, G. K.-L. Spin-Projected Matrix Product States: Versatile Tool for Strongly Correlated Systems. *J. Chem. Theory Comput.* **2017**, *13*, 2681−2695.
(85) Legeza, Ö.; Sólyom, J. Quantum Data Compression, Quantum Information Generation, and the Density-Matrix Renormalization-Group Method. *Phys. Rev. B: Condens. Matter Mater. Phys.* **2004**, *70*, 205118.

DOI: 10.1021/acs.jpclett.8b00503
J. Phys. Chem. Lett. 2018, 9, 1620−1626

(86) Chan, G. K.-L. An Algorithm for Large Scale Density Matrix Renormalization Group Calculations. *J. Chem. Phys.* **2004**, *120*, 3172−3178.
(87) Moritz, G.; Hess, B. A.; Reiher, M. Convergence Behavior of the Density-Matrix Renormalization Group Algorithm for Optimized Orbital Orderings. *J. Chem. Phys.* **2005**, *122*, 024107.
(88) Moritz, G.; Wolf, A.; Reiher, M. Relativistic Dmrg Calculations on the Curve Crossing of Cesium Hydride. *J. Chem. Phys.* **2005**, *123*, 184105.
(89) Rissler, J.; Noack, R. M.; White, S. R. Measuring Orbital Interaction Using Quantum Information Theory. *Chem. Phys.* **2006**, *323*, 519−531.
(90) Zgid, D.; Ghosh, D.; Neuscamman, E.; Chan, G. K.-L. A Study of Cumulant Approximations to N-Electron Valence Multireference Perturbation Theory. *J. Chem. Phys.* **2009**, *130*, 194107.
(91) Marti, K. H.; Reiher, M. The Density Matrix Renormalization Group Algorithm in Quantum Chemistry. *Z. Phys. Chem.* **2010**, *224*, 583−599.
(92) Chan, G. K.-L.; Sharma, S. The Density Matrix Renormalization Group in Quantum Chemistry. *Annu. Rev. Phys. Chem.* **2011**, *62*, 465−481.
(93) Schollwöck, U. The Density-Matrix Renormalization Group. *Rev. Mod. Phys.* **2005**, *77*, 259−315.
(94) Schollwöck, U. The Density-Matrix Renormalization Group in the Age of Matrix Product States. *Ann. Phys.* **2011**, *326*, 96−192.
(95) Hu, W.; Chan, G. K.-L. Excited-State Geometry Optimization with the Density Matrix Renormalization Group, as Applied to Polyenes. *J. Chem. Theory Comput.* **2015**, *11*, 3000−3009.
(96) Guo, S.; Watson, M. A.; Hu, W.; Sun, Q.; Chan, G. K.-L. N-Electron Valence State Perturbation Theory Based on a Density Matrix Renormalization Group Reference Function, with Applications to the Chromium Dimer and a Trimer Model of Poly(P-Phenylenevinylene). *J. Chem. Theory Comput.* **2016**, *12*, 1583−1591.
(97) Roemelt, M.; Krewald, V.; Pantazis, D. A. Exchange Coupling Interactions from the Density Matrix Renormalization Group and N-Electron Valence Perturbation Theory: Application to a Biomimetic Mixed-Valence Manganese Complex. *J. Chem. Theory Comput.* **2018**, *14*, 166−179.
(98) Ghosh, D.; Hachmann, J.; Yanai, T.; Chan, G. K.-L. Orbital Optimization in the Density Matrix Renormalization Group, with Applications to Polyenes and B-Carotene. *J. Chem. Phys.* **2008**, *128*, 144117.
(99) Sharma, S.; Chan, G. K.-L. Spin-Adapted Density Matrix Renormalization Group Algorithms for Quantum Chemistry. *J. Chem. Phys.* **2012**, *136*, 124121.
(100) Abegg, P. Ab Initio Calculation of Spin-Orbit Coupling Constants for Gaussian Lobe and Gaussian-Type Wave Functions. *Mol. Phys.* **1975**, *30*, 579−596.
(101) Hirata, S.; Head-Gordon, M. Time-Dependent Density Functional Theory within the Tamm−Dancoff Approximation. *Chem. Phys. Lett.* **1999**, *314*, 291−299.
(102) Tamm, I. Relativistic Interaction of Elementary Particles. *J. Phys.(USSR)* **1945**, *9*, 449.
(103) Dancoff, S. Non-Adiabatic Meson Theory of Nuclear Forces. *Phys. Rev.* **1950**, *78*, 382.
(104) Wong, B. M.; Hsieh, T. H. Optoelectronic and Excitonic Properties of Oligoacenes: Substantial Improvements from Range-Separated Time-Dependent Density Functional Theory. *J. Chem. Theory Comput.* **2010**, *6*, 3704−3712.
(105) Peach, M. J.; Williamson, M. J.; Tozer, D. J. Influence of Triplet Instabilities in Tddft. *J. Chem. Theory Comput.* **2011**, *7*, 3578−3585.
(106) Peach, M. J. G.; Tozer, D. J. Overcoming Low Orbital Overlap and Triplet Instability Problems in Tddft. *J. Phys. Chem. A* **2012**, *116*, 9783−9789.
(107) Sun, Q.; Berkelbach, T. C.; Blunt, N. S.; Booth, G. H.; Guo, S.; Li, Z.; Liu, J.; McClain, J. D.; Sayfutyarova, E. R.; Sharma, S. Pyscf: The Python-Based Simulations of Chemistry Framework. *Wiley Interdisciplinary Reviews: Computational Molecular Science* **2018**, *8*, e1340.
(108) Sayfutyarova, E. R.; Chan, G. K.-L., Electron Paramagnetic Resonance G-Tensors from State Interaction Spin-Orbit Coupling Density Matrix Renormalization Group. *arXiv preprint arXiv:1711.07195*, 2017.
(109) Peng, D.; Middendorf, N.; Weigend, F.; Reiher, M. An Efficient Implementation of Two-Component Relativistic Exact-Decoupling Methods for Large Molecules. *J. Chem. Phys.* **2013**, *138*, 184105.

DOI: 10.1021/acs.jpclett.8b00503
J. Phys. Chem. Lett. 2018, 9, 1620−1626